Effect of Chloride Anions on the Synthesis and Enhanced Catalytic Activity of Silver Nanocoral Electrodes for CO2 Electroreduction

ARTICLE *in* ACS CATALYSIS · JULY 2015

Impact Factor: 9.31 · DOI: 10.1021/acscatal.5b01235

5 AUTHORS, INCLUDING:

Sanjaya D. Senanayake

Brookhaven National Laboratory

108 PUBLICATIONS **1,703** CITATIONS

SEE PROFILE

Yu Zhang

Brookhaven National Laboratory

11 PUBLICATIONS **204** CITATIONS

SEE PROFILE

Wenqian Xu

Brookhaven National Laboratory

53 PUBLICATIONS **554** CITATIONS

SEE PROFILE

Dmitry E Polyansky

Brookhaven National Laboratory

40 PUBLICATIONS **681** CITATIONS

SEE PROFILE

ACS Catalysis

Research Article

pubs.acs.org/acscatalysis

Effect of Chloride Anions on the Synthesis and Enhanced Catalytic Activity of Silver Nanocoral Electrodes for CO_2 Electroreduction

Yu-Chi Hsieh, Sanjaya D. Senanayake, Yu Zhang, Wenqian Xu,[†] and Dmitry E. Polyansky*

Chemistry Department, Brookhaven National Laboratory, Upton, New York 11973-5000, United States

Supporting Information

ABSTRACT: Metallic silver (Ag) is known as an efficient electrocatalyst for the conversion of carbon dioxide (CO_2) to carbon monoxide (CO) in aqueous or nonaqueous electrolytes. However, polycrystalline silver electrocatalysts require significant overpotentials in order to achieve high selectivity toward CO_2 reduction, as compared to the side reaction of hydrogen evolution. Here we report a high-surface-area Ag nanocoral catalyst, fabricated by an oxidation−reduction method in the presence of chloride anions in an aqueous medium, for the electro-reduction of CO_2 to CO with a current efficiency of 95% at the low overpotential of 0.37 V and the current density of 2 mA cm^{-2}. A lower limit of TOF of 0.4 s^{-1} and TON > 8.8 × 10^4 (over 72 h) was estimated for the Ag nanocoral catalyst at an overpotential of 0.49 V. The Ag nanocoral catalyst demonstrated a 32-fold enhancement in surface-area-normalized activity, at an overpotential of 0.49 V, as compared to Ag foil. We found that, in addition to the effect on nanomorphology, the adsorbed chloride anions play a critical role in the observed enhanced activity and selectivity of the Ag nanocoral electrocatalyst toward CO_2 reduction. Synchrotron X-ray photoelectron spectroscopy (XPS) studies along with a series of control experiments suggest that the chloride anions, remaining adsorbed on the catalyst surface under electrocatalytic conditions, can effectively inhibit the side reaction of hydrogen evolution and enhance the catalytic performance for CO_2 reduction.

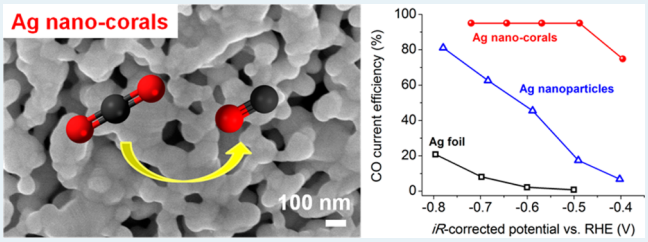

KEYWORDS: *nanoporous Ag, chloride modification, carbon dioxide reduction, electrocatalysis, high selectivity*

INTRODUCTION

Decreasing the accumulation of carbon dioxide (CO_2) in Earth's atmosphere is one of the most important issues for human society on the path to develop sustainable technology and protect the environment.[1,2] Electrochemical reduction of CO_2 has received wide attention and is considered as a promising method for synthesizing carbon-containing fuels and achieving sustainable energy conversion and storage.[3−14] However, one of the major drawbacks of electrochemical CO_2 reduction in aqueous solution is the high overpotential required to achieve substantial reaction rates and selectivity.[11,15−17] The origin of high overpotential was proposed by Bockris et al.[15,16] to be the formation of $CO_2^{\bullet-}$ as the first reaction intermediate. The very negative reduction potential of the $CO_2/CO_2^{\bullet-}$ couple, E° = −1.9 V vs standard hydrogen electrode (SHE),[17,18] creates a significant thermodynamic and kinetic bottleneck for the overall CO_2 reduction reaction. In addition to the associated energy loss, the use of more negative potentials increases the efficiency of other side reactions, for example the hydrogen evolution reaction (HER), and thus decreases the current efficiency of the CO_2 reduction reaction.

A catalyst's performance can be evaluated using three key factors: its activity, selectivity, and durability. High activity is characteristic to catalysts that operate at low overpotential and exhibit large current for the electrocatalytic reaction. Selectivity refers to the yield of the main product over that of side products. Under the reaction conditions for CO_2 electroreduction in aqueous solutions, the major side reaction is the HER. Finally, the durability characterizes a catalyst's ability to maintain its initial activity over an extended operation time with little or no degradation. Among others, three transition metals: Cu,[5,13,19−23] Ag,[24−29] and Au[19,30−32] have been most extensively studied as electrocatalysts for the CO_2 reduction reaction. Hori reported that Cu, Ag, and Au had high activities for CO_2 reduction at potentials of −1.04, − 0.97, and −0.74 V (vs reversible hydrogen electrode, RHE), respectively,[17] with a current density of −5 mA cm^{-2} in 0.1 M $KHCO_3$. However, Cu demonstrated poor selectivity, resulting in the formation of a variety of products. While Au was reported to operate at the lowest overpotential among these three metals and showed a high selectivity for CO_2 reduction to carbon monoxide (CO),[30,32] its substantial cost may limit potential industrial applications.

The electroreduction of CO_2 on flat Ag surfaces was shown to produce CO with a reasonably high selectivity (~90%), but at substantially high overpotentials,[24,33] with respect to the standard reduction potential E° = −0.106 V (vs SHE) of the reaction $CO_2 + 2H^+ + 2e^- = CO + H_2O$.[11] In order to further

Received: December 8, 2014
Revised: July 29, 2015

DOI: 10.1021/acscatal.5b01235
ACS Catal. 2015, 5, 5349−5356

enhance the CO_2 reduction activity of Ag, nanostructured Ag-based catalysts with increased surface area have been developed.[26−28] A 10-fold increase in the intrinsic activity was achieved by 5 nm Ag nanoparticles compared to bulk Ag.[28] Nanoporous Ag prepared by the dealloying method showed 92% selectivity for CO_2 reduction to CO at a moderate overpotential of 0.49 V, and a 20 times higher intrinsic activity than bulk Ag.[26] The enhanced activity of the nanostructured Ag catalysts was attributed to the greater stabilization of $CO_2^{\bullet-}$ on the nanoporous Ag.[26]

In this work, we fabricated a nanostructured coral-like Ag electrocatalyst, via an oxidation−reduction process using chloride anions. The Ag nanocoral catalyst exhibited a high activity for CO_2 reduction with a low overpotential of 0.37 V, and a high selectivity with a CO current efficiency of 95%. The Ag nanocorals displayed a 660-fold enhancement in CO partial current density compared to bulk Ag, which corresponds to a 32-fold improvement in intrinsic activity, along with a 20-fold increase of electrochemical surface area. We found that the effect of chloride anions was more than facilitating the fabrication of the high-surface-area nanostructured Ag catalyst. More importantly, the presence of chloride anions on the catalyst surface plays a crucial role in the performance enhancement for the CO_2 reduction reaction, by enhancing the intrinsic activity for CO_2 reduction, and by improving the selectivity for the product CO by suppressing the side HER. The long-term durability of the Ag nanocoral catalyst was evaluated, and the possible reason for the performance degradation is discussed.

EXPERIMENTAL SECTION

Materials. Silver foil (99.9985%, 0.5 mm thick, Alfa Aesar) was used following the cleaning procedure described below. Potassium bicarbonate ($KHCO_3$, 99.7%, Baker Analyzed) and potassium chloride (KCl, 99.1%, Baker Analyzed) were used to prepare the electrolytes. The 0.1 M $KHCO_3$ solution was purified by pre-electrolysis, where the solution was saturated with Ar, and Pt foil (24.6 cm^2) was used as the working electrode at an applied potential to maintain a constant current of −10 mA for 12 h. The 0.1 M KCl solution was also pre-electrolyzed using a similar method. Deionized water (purified by a Milli-Q system) was used to prepare all solutions and to rinse samples and glassware.

Sample Preparation. The Ag foil was cleaned by immersion and sonication for 15 min sequentially in hexane (99.9%), ethanol, and then deionized water. The AgCl sample was prepared by oxidizing Ag foil in 0.1 M Ar-saturated pre-electrolyzed KCl solution at 0.3 V (vs Ag/AgCl, 3 M KCl) for 12 h and then rinsing. The Ag nanocoral sample was prepared by reducing the as-prepared AgCl in 0.1 M CO_2-saturated pre-electrolyzed $KHCO_3$ solution at −1.2 V (vs Ag/AgCl, 3 M KCl) for 30 min and then rinsing. After the reduction process, the electrochemical cell was thoroughly rinsed and filled with fresh 0.1 M pre-electrolyzed $KHCO_3$ solution purged with CO_2 to perform the CO_2 reduction reaction.

Synthesis of Ag Nanoparticles (NPs). 1 g of $AgNO_3$ was dissolved in 100 mL of deionized water, and 500 mg of sodium citrate was dissolved in another 100 mL of deionized-water. The two solutions were mixed together and stirred for 30 min. A solution of 1 g of $NaBH_4$ in 50 mL of deionized water was quickly added into the reaction solution, and the mixture was stirred for 2 h. Then the solution was filtered and the precipitate was rinsed repeatedly with deionized water to remove any remaining byproducts, until the pH of the filtered liquid reached 7. The filtered Ag nanoparticles were then added into 250 mL of deionized water, and the mixture was sonicated for 2 h. After that, the suspension was centrifuged at 3000 rpm for 1 h, and the clear supernatant with a yellow−green color was collected in order to remove the larger nanoparticles. Then the yellow-green supernatant was centrifuged at 9000 rpm for 1 h, and the solid sediment was collected in order to separate from smaller nanoparticles. The collected Ag nanoparticles were redispersed in water and then deposited onto clean pure Ag foil. After drying, the Ag foil with Ag nanoparticles was baked at 200 °C for 1 h and then immersed in acid, in order to remove impurities on the nanoparticle surface. The nanoparticle loading for electrochemical measurements was 1.2 mg cm^{-2} Ag. The average particle size of the Ag NPs (50 ± 24 nm) was measured by SEM (Figure S1) using Image-Pro Plus software.

Electrochemical Methods. An EC-epsilon BASi potentiostat was used for all electrochemical experiments. Pt gauze was used as the counter electrode. The reference electrode was a Ag/AgCl (3 M KCl, BASi) electrode unless otherwise noted, with the potential deviation of 0.13 mV.[34] The reference electrode was periodically calibrated against the hydrogen reference electrode (Hydroflex, eDAQ), and the environmental temperature variations (±5 °C) resulted in uncertainties in reference potentials of ca. ±1 mV. The potentials were measured against the reference electrode and converted to the reversible hydrogen electrode (RHE) reference scale by $E_{RHE} = E_{Ag/AgCl} + 0.197 + 0.059pH_{electrolyte}$. All the potentials were reported versus RHE unless otherwise noted. Electrochemical impedance spectroscopy was used to determine the high frequency resistance (HFR) as the uncompensated solution resistance (R_u) at AC frequency ranging from 10 MHz to 1 Hz. The HFR was measured at −0.3 and −1.5 V where its values at the two potentials differ by only 0.1 Ω, and the average value was used. The potential was corrected using automatic *iR* compensation function of the potentiostat by applying 85% of the R_u value measured using impedance spectroscopy. The use of this value ensured the stable operation of the potentiostat.[35] The remainder 15% of the R_u was mathematically corrected, using the following equation:[24]

$$E_{100\%iR\text{-corrected}} = E_{85\%iR\text{-corrected}} - 15\% \times \text{average } R_u \times \text{average } i$$

where $E_{100\%iR\text{-corrected}}$ is the final reported potential; $E_{85\%iR\text{-corrected}}$ is the potential used in the controlled potential electrolysis experiment with the *iR* compensation function using 85% of R_u; average *i* is the average current attained by averaging the total electric charge over the duration of the controlled potential electrolysis experiment.

The electrochemical surface area was determined using lead (Pb) underpotential deposition (UPD) in 1 mM $Pb(acetate)_2$ + 1 mM $HClO_4$ + 0.5 M $NaClO_4$ solution, at 10 mV s^{-1}. A saturated calomel electrode (SCE) was used as the reference electrode. As shown in Figure S2, the Pb UPD desorption peak at −0.35 to −0.2 V (vs SCE) was integrated to calculate the electrochemical surface area, assuming 420 $\mu C\ cm_{ec}^{-2}$ for Ag-based samples.[36,37]

CO_2 Reduction Measurements and Product Analyses. The custom-designed electrochemical cell consisting of three gastight compartments (for the working, counter, and reference electrodes respectively) was used in electrocatalytic experi-

DOI: 10.1021/acscatal.5b01235
ACS Catal. 2015, 5, 5349−5356

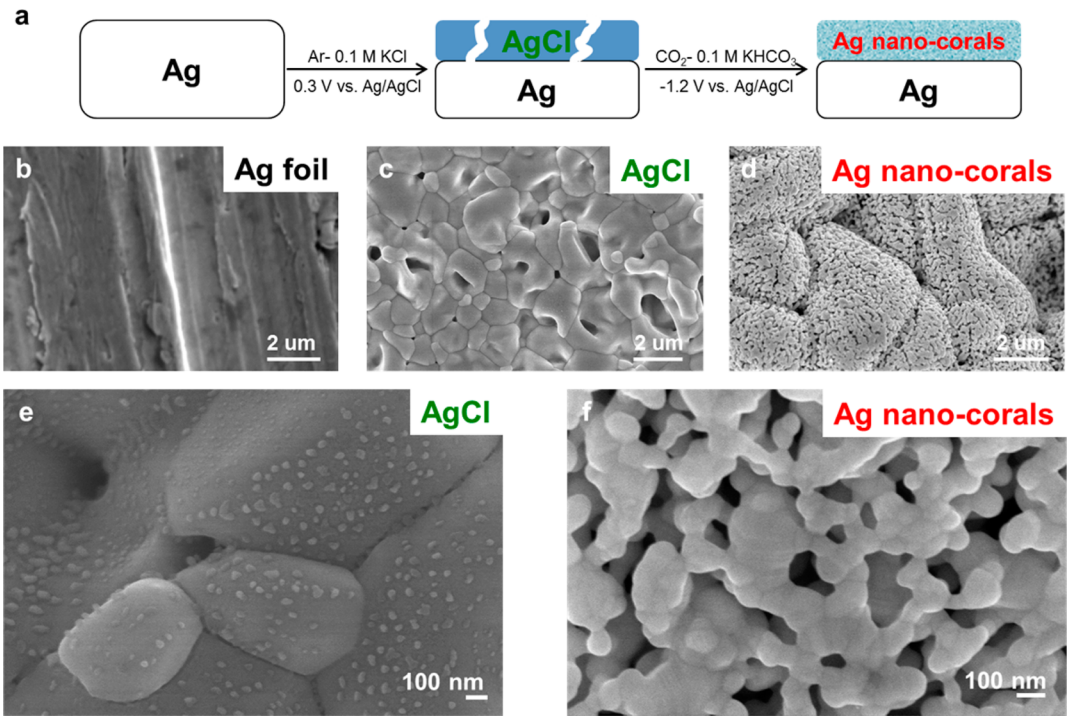

Figure 1. (a) Schematic illustration of the formation of as-prepared AgCl and Ag nanocorals. SEM images of (b) untreated Ag foil, (c) as-prepared AgCl after 12 h oxidation, and (d) Ag nanocorals. High-magnification SEM images of (e) as-prepared AgCl after 12 h oxidation and (f) Ag nanocorals.

ments. The working and counter compartments contained 12 mL electrolyte each with 14.8 mL headspace. The compartment for the working electrode was separated from the counter electrode compartment by a glass frit with porosity sufficient to prevent the diffusion of Pt species produced by dissolution of the counter electrode under the experimental conditions, as well as to prevent the diffusion of products produced at the working electrode to the counter electrode compartment. The reference electrode compartment was connected to the working electrode compartment through a capillary.

The CO_2 reduction reaction was carried out in CO_2-saturated 0.1 M pre-electrolyzed $KHCO_3$ (pH = 6.8, measured by an Accumet AB15 pH meter) at different potentials for 30 min, while the electrolyte was stirred at 870 rpm. Upon the completion of electrolysis, a 60 μL gas sample was removed through a septum port via a gastight syringe and was injected into a gas chromatograph (GC) instrument (Agilent 6890N) to quantify the amount of CO and H_2. For the as-prepared AgCl sample (Supporting Information Figure S3), the catalytic performance was measured in CO_2-saturated 0.1 M pre-electrolyzed $KHCO_3$ (pH = 6.8) at −0.6 V for 2 h and a 60 μL gas sample was taken every 15 min into the GC for product analysis. The solution-phase products were analyzed by ion chromatography (Thermo-Fisher Dionex ICS-1600).

The durability test of CO_2 reduction was carried out in CO_2-saturated 0.1 M pre-electrolyzed $KHCO_3$ at −0.6 V for 72 h. After the 72 h durability test, the electrochemical cell was thoroughly rinsed, and fresh 0.1 M pre-electrolyzed $KHCO_3$ solution was filled and purged with CO_2 to perform the CO_2 reduction reaction at −0.6 V for 30 min.

Characterization. The soft X-ray photoelectron spectroscopy (sXPS) experiments were conducted at the National Synchrotron Light Source (NSLS, BNL) at the U12A beamline. The end-station at this beamline is an ultrahigh-vacuum (UHV) chamber (1×10^{-10} Torr) equipped with a hemispherical analyzer for photoemission and is described in detail elsewhere.[38] The incident photon energy for all measurements was 600 eV at an energy resolution of 0.3 eV. Energy calibration was performed for all sXPS spectra using the corresponding position of the adventitious carbon feature in the C 1s peak at 284.6 eV, with cross reference with the Fermi edge of the Cu sample mount (0 eV). The X-ray diffraction (XRD) experiments were conducted at the National Synchrotron Light Source (NSLS, BNL) at the X7B beamline. The wavelength was 0.3196 Å. The Rietveld refinements were performed using the GSAS software to estimate the grain size (Supporting Information Figure S4 and Table S1). Scanning electron microscopy (SEM) images were obtained using a Hitachi 4800 scanning electron microscope at the Center for Functional Nanomaterials (CFN) at BNL. The atomic ratio of Ag to Cl was determined by X-ray photoelectron spectroscopy (XPS) measurements using an RHK Technology UHV 7500 with monochromatized Al Kα radiation (1486.7 eV) at the Center for Functional Nanomaterials (CFN) at BNL and by energy-dispersive X-ray spectroscopy (EDS) measurements using an Ametek EDAX silicon drift detector (SDD) equipped on a Hitachi S-3400N SEM.

RESULTS AND DISCUSSION

Synthesis and Characterization of Ag Nanocorals. Nanostructured coral-like Ag samples were fabricated by subjecting a Ag foil to an oxidation−reduction process in the presence of Cl^-. A schematic illustration of the synthetic process is depicted in Figure 1a, and the SEM images (Figures 1b−d) show the corresponding changes to the surface morphology. First, during the oxidation in Ar-saturated 0.1 M KCl, an anodic potential is applied to pure Ag foil (Figure 1b) which oxidizes Ag surface atoms to form Ag^+ in the solution

DOI: 10.1021/acscatal.5b01235
ACS Catal. 2015, 5, 5349−5356

phase, followed by the interaction of Ag^+ with Cl^- to form solid AgCl (Figure 1c) on the Ag surface.[39,40] With prolonged oxidation of the Ag foil, the AgCl formed on the Ag surface exhibits a dense structure with microchannels (as shown schematically in Figure 1a). In the next step, the surface layer of AgCl is reduced in CO_2-saturated 0.1 M $KHCO_3$. Under cathodic potential, AgCl decomposes into equal amounts of Ag^+ and Cl^- near the electrode surface. The Ag^+ cations are reduced to Ag atoms, and subsequently the Ag atoms nucleate and are deposited back onto the substrate, while Cl^- anions diffuse into the electrolyte.[40,41] These reactions convert the dense AgCl (Figure 1c and e) into a coral-like nanoporous Ag sample (denoted as "Ag nanocorals", Figure 1d and f) with the pore size depending on the Ag nucleation rate determined by the reduction current density.[40] Synchrotron XRD measurements were carried out to investigate the crystal structure of these Ag-based samples (Figure S4, Table S1). Ag foil showed a face-centered cubic (fcc, space group 225, $Fm\bar{3}m$) structure. The as-prepared AgCl sample exhibited two phases, including the AgCl(fcc) phase lying on the surface and metallic Ag(fcc) phase due to the substrate, and therefore two sets of fcc peaks from Ag and AgCl can be found in the diffractogram. In contrast, the Ag nanocorals displayed only one set of Ag(fcc) peaks, and the absence AgCl(fcc) peaks was probably due to the very small amount of Cl^- left on the catalyst surface after the oxidation–reduction process (vide infra).

In order to investigate the surface composition and chemical states of the Ag nanocorals, the surface-sensitive soft X-ray photoelectron spectroscopy (sXPS) measurements were performed at a synchrotron beamline. First, an XPS survey in a wide energy range (Figure 2a) was carried out, and the peaks

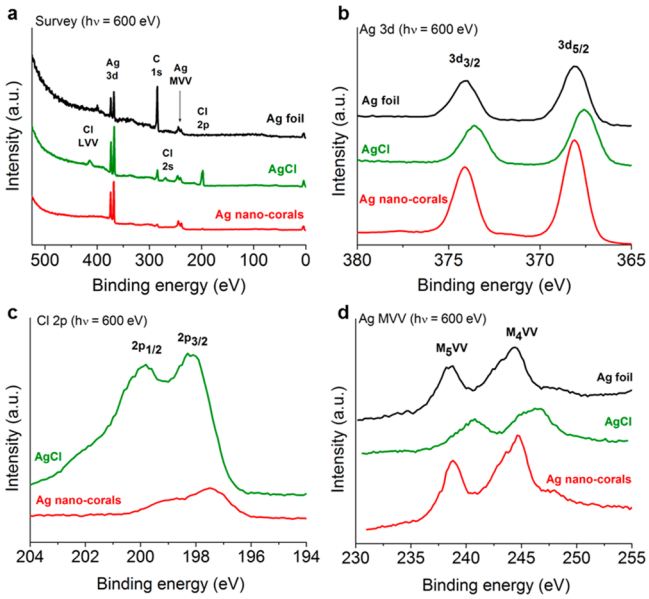

Figure 2. Synchrotron sXPS spectra of (a) survey, (b) Ag 3d, (c) Cl 2p, and (d) Ag MVV for Ag foil (black), as-prepared AgCl (olive green), and Ag nanocorals (red).

of Ag, Cl, and C were identified. The adventitious C 1s peak was used for energy scale calibration. A higher resolution scan of the Ag 3d region is presented in Figure 2b. The two bands at 368.1 and 374 eV can be attributed to the Ag $3d_{5/2}$ and Ag $3d_{3/2}$ binding energies, respectively. According to the literature values, the Ag metallic state (Ag^0) exhibit two peaks at 368.2 and 374.2 eV and AgCl sample (Ag^+) has peaks at 367.2 and 373.2 eV, respectively.[42−44] The Ag nanocoral sample (red) has a similar Ag 3d band structure to the Ag foil (black). Figure 2c shows the Cl 2p region including the $2p_{1/2}$ and $2p_{3/2}$ features. In the AgCl sample (olive green), Cl and Ag are chemically bonded with a 1:1 atomic ratio (Figure 2c and d) and form an ordered rock-salt crystal structure (Figure S4). For the Ag nanocoral sample (red), Cl forms a stable chemically bonded thin layer on the Ag surface in the Cl^- state, instead of entering the Ag lattice.[45] The Cl 2p peaks of the Ag nanocorals (red) are red-shifted by 0.8−1.1 eV compared to those of the AgCl (olive green) due to an imbalanced surface charge. The bonding between the surface Cl^- species and the Ag surface atoms is very stable for Ag nanocorals,[39,46] as demonstrated by the high desorption temperature of 700 K for the surface Cl^- species on Ag.[46]

The Ag foil and Ag nanocorals show similar Ag 3d structure, but their corresponding Ag MVV auger transitions exhibit different peak positions and densities (Figure 2d). The Ag MVV spectra are shown using a binding energy scale, but in the numeric direction opposite to convention in order to facilitate the comparison with literature results. MVV energies were calibrated using the adventitious C 1s at 284.6 eV, since the surface work function (ϕ) was not accurately accessible. The energy shift of the Ag M_4VV peak for as-prepared AgCl compared to that for Ag foil was 2.3 eV (Table 1), which is

Table 1. Binding Energies (eV) from XPS Measurements of Various Ag Electrocatalysts Studied in This Work

	Ag $3d_{5/2}$	Ag $3d_{3/2}$	Ag M_5VV	Ag M_4VV	Cl $2p_{3/2}$	Cl $2p_{1/2}$
Ag foil	368.1	374.0	244.4	238.4		
As-prepared AgCl	367.5	373.6	246.3	240.7	198.2	199.8
Ag nanocorals	368.1	374.1	244.7	238.7	197.4	198.7
Ag nanocorals, 72 h CO_2 reduction	367.4	373.4	241.5	235.7	197.8	199.3

consistent with the reported value of a 2.5 eV shift between these two samples.[47,48] It should be noted that for the Ag nanocoral sample after the oxidation–reduction process in the presence of the chloride anions, both of its Ag MVV peaks shifted by 0.3 eV, compared with Ag foil, suggesting that the Ag nanocoral sample contained a small amount of Ag^+ on the Ag surface. The analyses of Ag MVV and Cl 2p peaks of the Ag nanocoral sample suggest that a small amount of Ag^+ bound to Cl^- is retained on the catalyst surface, which may be the active species contributing to the high activity and selectivity of the Ag nanocorals toward CO_2 reduction.

Performance for CO_2 Reduction. The CO_2 reduction activity was evaluated at constant potentials in CO_2-saturated 0.1 M $KHCO_3$. The gaseous products and the solution-phase products were analyzed by gas chromatography (GC), and by ion chromatography (IC), respectively. First, we assessed the activity of as-prepared AgCl at −0.6 V (vs RHE) as shown in Figure S3. Within 25 min from the beginning of electrolysis, high current densities were observed, although the current efficiencies for both CO and H_2 were close to zero, indicating that the observed currents were dominated by the reductive decomposition of AgCl. After 45 min of electrolysis, the CO current efficiency increased rapidly and reached 95%, while the H_2 current efficiency stabilized below 1.5%, and the only solution-phase product that could be accurately detected was

DOI: 10.1021/acscatal.5b01235
ACS Catal. 2015, 5, 5349−5356

formate ($HCOO^-$) with 1−2% current efficiency. It is informative to compare the CO_2 reduction activity of the Ag nanocoral sample, pure Ag foil and Ag nanoparticles (Ag NPs) as shown in Figure 3. The Ag foil exhibited very low CO current efficiency (2−12%) and high H_2 current efficiency (60−90%) at potentials ranging from −0.5 to −0.8 V.[24−26,33] In stark contrast, the Ag nanocoral sample demonstrated very high CO current efficiencies reaching 95%, and very low H_2 current efficiency (<2%), at potentials below −0.6 V, indicating excellent selectivity for CO_2 reduction to CO. The Ag NPs (50 ± 24 nm) showed higher CO_2 reduction activity compared to Ag foil as a result of the nanosize effect which provided an enhanced surface area and higher intrinsic activity. The CO partial current densities for the Ag nanocorals and Ag NPs were 660 times and 40 times, respectively, higher as compared to Ag foil.

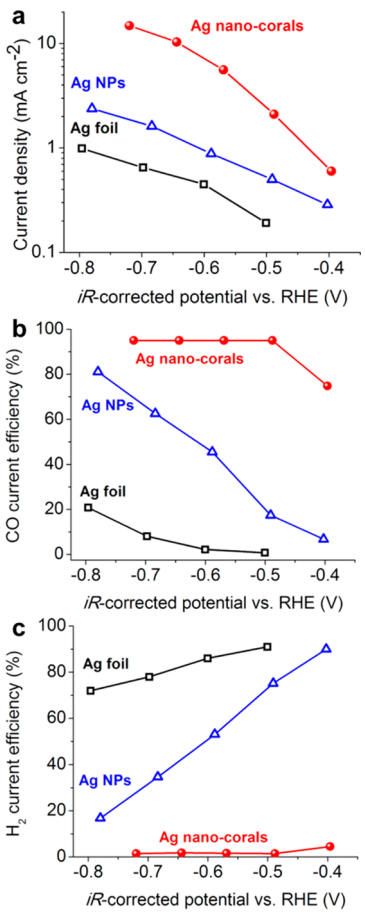

Figure 3. (a) Total current density, (b) CO current efficiency, and (c) H_2 current efficiency, measured in CO_2-saturated 0.1 M $KHCO_3$ at different potentials (*iR*-corrected), for Ag foil (hollow black square), Ag nanoparticles (NPs, hollow blue triangle), and Ag nanocorals (red sphere).

The CO partial current density was normalized by the electrochemical surface area, determined by the Pb underpotential deposition (UPD) method (shown in Figure S2), to calculate the specific activity (SA in Table 2). Specific activity excludes the influence of different surface areas, and therefore it can be used to represent the intrinsic activity of catalysts. Ag nanocorals demonstrated the highest specific activity of 162 μA cm^{-2}, which was 32 times higher than that of Ag foil (5 μA cm^{-2}), and was 7 times greater than the specific activity of the Ag nanoparticles (21.6 μA cm^{-2}). Despite the larger particle size, Ag nanocorals (~150 nm, Table S1) exhibit substantially higher specific activity as compared to Ag nanoparticles (50 ± 24 nm, shown in Figure S1), suggesting that the effect of nanostructured morphology is not the sole contributor to the CO_2 reduction performance. We propose that the surface bound chloride ions (or associated surface silver ions) are responsible for the higher activity and selectivity of AgCl-derived Ag nanocorals toward electro-reduction of CO_2 to CO.

Table 2. CO_2 Reduction Performance on Ag Foil, Ag Nanocorals, and Ag Nanoparticles[a]

	j_{CO} (μA cm$_{geo}^{-2}$)	A_{ec} (cm$_{ec}^2$)	SA (μA cm$_{ec}^{-2}$)	CO current efficiency (%)
Ag foil	10	2	5	2.2
Ag nanocorals	6620	40.8	162	95.0
Ag NPs	400	18.5	21.6	45.4

[a]The term j_{CO} is the CO partial current density calculated by multiplying the CO current efficiency by the measured current density (normalized by the electrode geometric area, A_{geo} = 1 cm^2). A_{ec} is the electrochemical surface area measured by the Pb UPD method (Figure S2). SA is the specific activity where SA = $j_{CO}A_{geo}/A_{ec}$. The j_{CO} and CO current efficiency were measured at −0.6 V (vs RHE with *iR*-correction).

Furthermore, Tafel analysis was performed to gain mechanistic insights[49] for the CO_2 reduction on the Ag-based catalysts' surface. It is commonly considered that the initial step in the overall two-electron reduction of CO_2 to CO on most metal surfaces is a one-electron transfer step forming adsorbed $CO_2^{\bullet-}$:

$$CO_2 + e^- \rightarrow CO_{2ads}^{\bullet-} \quad (1)$$

The standard reduction potential for the $CO_2/CO_{2ads}^{\bullet-}$ couple is very negative (E^0 = −1.9 V vs SHE)[17,18] but can be shifted toward more positive values due to specific interactions between the adsorbed $CO_2^{\bullet-}$ radical and the surface atoms of a metal electrode.[50]

Next, the reaction intermediate $CO_{2ads}^{\bullet-}$ reacts with two protons and gains another electron to form CO:[17,51]

$$CO_{2ads}^{\bullet-} + HCO_3^- \rightarrow COOH_{ads} + CO_3^{2-} \quad (2)$$

$$COOH_{ads} + HCO_3^- + e^- \rightarrow CO_{ads} + H_2O + CO_3^{2-} \quad (3)$$

$$CO_{ads} \rightarrow CO \quad (4)$$

Step 2 is a chemical step involving protonation of $CO_{2ads}^{\bullet-}$ to form $COOH_{ads}$ intermediate.[52] Under experimental conditions similar to those described in this work, HCO_3^- is the most likely source of protons, since the pK_a of bicarbonate is much lower as compared to that of water.[51] Step 3 is an electrochemical step coupled to a chemical reaction involving proton and electron transfer, and step 4 is the desorption of CO product.

As shown in Figure 4, the polycrystalline Ag foil exhibited a Tafel slope of 137 mV dec^{-1}, which is close to 140 mV dec^{-1} for polycrystalline Ag under similar experimental conditions[24] and comparable to 132 mV dec^{-1} measured in 0.5 M $KHCO_3$.[26] The Tafel slope of 137 mV dec^{-1} for polycrystalline Ag foil in our experiments was also close to the value of 130 mV dec^{-1} for polycrystalline Au.[17] These results indicate that polycrystalline Ag and Au could have the same rate-determining

DOI: 10.1021/acscatal.5b01235
ACS Catal. 2015, 5, 5349−5356

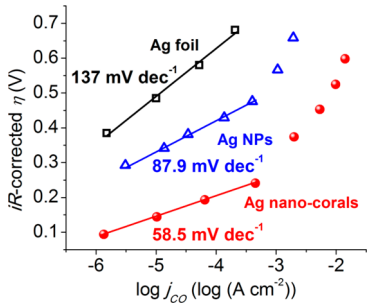

Figure 4. Tafel plot at different overpotentials η (*iR*-corrected) as a function with the CO partial current density j_{CO}, on Ag foil (hollow black square), Ag NPs (hollow blue triangle), and Ag nanocorals (red sphere).

step, which was assigned previously to the one-electron reduction of CO_2 to form $CO_{2ads}^{\bullet-}$ eq 1 with the theoretical Tafel slope of 118 mV dec^{-1}.[17,24,26,30] In contrast, in our experiments Ag nanoparticles showed a Tafel slope of 87.9 mV dec^{-1}, indicating that the reaction kinetics is faster as compared to Ag foil and the rate-determining step is not pure electron transfer.[26,51]

Interestingly, the Ag nanocoral sample displayed the lowest Tafel slope of 58.5 mV dec^{-1}, indicating that the reaction kinetics on Ag nanocorals is the fastest among these samples. Similar Tafel slopes of 56−58 mV dec^{-1} were also reported for oxide-derived Au[30] and for nanoporous Ag.[26] The Tafel slope for Ag nanocorals is very close to the theoretical value of 59 mV dec^{-1}, suggesting that a chemical step (such as in eq 2) is the rate-determining, followed by another electron transfer.[51,53,54] The effects of halides present at the electrode surface or in the electrolyte have been previously reported for CO_2 electroreduction on copper surfaces,[55] and substantial improvement in current efficiency and selectivity was observed. It appears that the presence of chloride ions on the Ag electrode surface or in the electrolyte solution in proximity to the electrode promotes selectivity and activity for the CO_2 reduction reaction.

In an attempt to further confirm the role of the surface chloride in CO_2 electroreduction, the AgCl-derived nanocoral catalyst was subjected to a reductive treatment under hydrogen atmosphere, in order to remove the adsorbed Cl from the Ag surface while retaining the porous structure (see the Supporting Information for details). The reduced sample shows a relatively low CO current efficiency of 41% and high H_2 current efficiency of 58%, as compared to a 95% current efficiency for the nanocoral Ag catalyst under similar experimental conditions (Supporting Information Figure S5). However, addition of Cl^- to the electrolyte solution leads to an increase in CO current efficiency even without the oxidation/reduction treatment; though only up to ca. 63% (Supporting Information Figure S5c). In order to quantify the effect of the Cl surface coverage on the electrocatalytic performance, the correlation between the amount of surface chloride and the CO_2 reduction activity was investigated. Ag NPs deposited on silver foil supports were used as substrate material in order to attain controllable chloride concentration and maintain the constant catalysts' surface area. Ag NPs were immersed in HCl solution for different periods of time, and the atomic ratio of Cl:Ag on NPs' surface was determined by XPS measurements. With the prolonged immersion in 3.5 wt % HCl solution the Cl:Ag ratio increases, together with an increase in CO partial current density (Supporting Information Figure S6a). The Ag NPs immersed in HCl solution for 4 h exhibit the highest Cl:Ag ratio and therefore the best CO_2 reduction performance within the sample series. Compared to unmodified Ag NPs, the Ag NPs immersed for 4 h demonstrate a 4.5-fold enhancement in CO partial current density and a 4.7-fold enhancement in specific activity, and the CO current efficiency rise from 43% to 74%, while the surface morphology remains virtually unaffected (Supporting Information Figure S6b). In summary, these experiments confirm that the presence of chloride on the electrode surface or in the proximity of the solid-solution interface beneficially impacts the selectivity and activity of the CO_2 electroreduction reaction.

The long-term stability of the Ag nanocorals under catalytic conditions was investigated by performing CO_2 reduction at −0.6 V for 72 h. It was found that upon completion of the test, the surface morphology changed from a coral-like to a dendrite-like structure (Figure 5a and b). As a result, both the

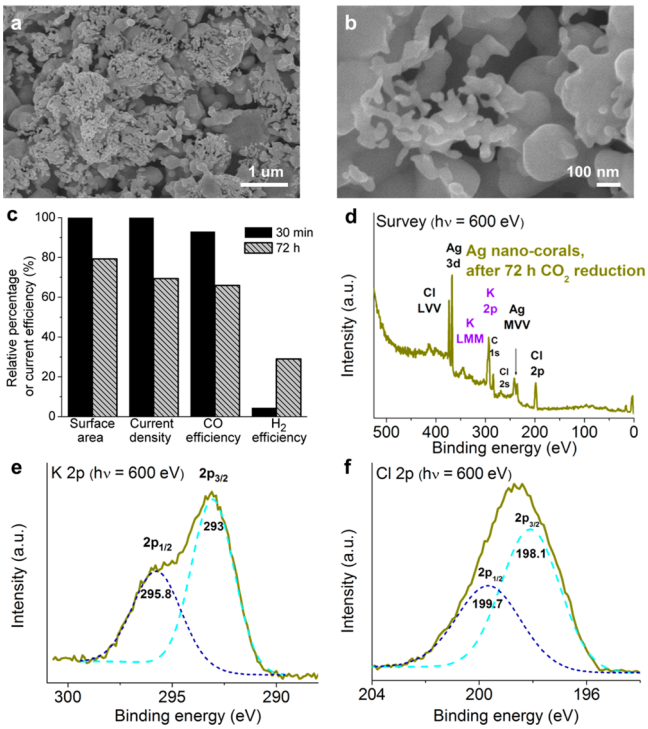

Figure 5. (a) Low- and (b) high-magnification SEM image of the Ag nanocorals after 72 h CO_2 reduction. (c) Comparison of CO_2 reduction activity for the Ag nanocorals after 30 min (solid black) and 72 h (striped gray) CO_2 reduction at −0.6 V (with *iR*-correction). Surface area and current density are shown in relative percentage (%). XPS spectra of (d) survey, (e) K 2p, and (f) Cl 2p for the Ag nanocorals after 72 h CO_2 reduction (dark yellow).

electrochemical surface area and the current density dropped by 20% and 30%, respectively, and the CO current efficiency decreased from 95% to 66%, while the H_2 efficiency increased from 1.7% to 29% after 72 h of CO_2 reduction (striped gray, Figure 5c), compared to that after 30 min of reduction (solid black, Figure 5c). Alternatively, the nanocoral catalyst's stability can be measured in terms of turnover number (TON). The TON of the Ag nanocoral catalyst is estimated to be 720 over 30 min or 8.8×10^4 over 72 h, with the turnover frequency (TOF) estimated as 0.4 s^{-1}, based on the ratio of the number of CO_2 molecules reduced per unit time to the number of surface silver atoms (see the Supporting Information for details). These

DOI: 10.1021/acscatal.5b01235
ACS Catal. 2015, 5, 5349−5356

estimates represent a lower limit, due to the assumption that all surface Ag atoms are catalytically active.

We have also considered the possibility of contamination of working electrodes by electrodeposited Pt ions, which can be produced through dissolution of oxidized Pt counter electrode and Pt ion crossing to the working electrode compartment. It is known that the Pt counter electrode can undergo significant oxidation and dissolution,[56,57] generating Pt(II) and Pt(IV) species in the electrolyte,[58] which may subsequently diffuse to and be deposited at the working electrode. Such Pt deposit could consequently cause a change in the activity of the working electrode.[49,59] In our CO_2 reduction measurements, the working electrode compartments and the counter electrode compartment were separated by a glass frit with an appropriate porosity to prevent the diffusion of dissolved Pt species to the working electrode. This was confirmed by placing solutions of various Pt species (e.g., $PtCl_6^{2-}$) in the counter electrode compartment and pure water in the working electrode compartment and monitoring the UV−vis absorbance of both solutions. No Pt ions crossover was observed over the time frame of ca. 72 h. In addition, XPS spectra of Ag nanocoral samples exhibited no observable Pt signals (Pt 4f) either after 30 min or after 72 h of CO_2 reduction (Supporting Information Figure S7). The absence of Pt signals shows that the diffusion of dissolved Pt species has been effectively blocked by the glass frit between working and counter electrode compartments.

It is noteworthy that the XPS analysis of the sample after 72 h of CO_2 reduction (Figure 5d) indicated the presence of potassium (K) atoms on the surface. The K 2p signal is analyzed and fitted with two peaks corresponding to $2p_{1/2}$ at 295.8 eV and $2p_{3/2}$ at 293 eV (Figure 5e). The Cl 2p signal is fitted with two peaks due to $2p_{1/2}$ at 199.7 eV and $2p_{3/2}$ at 198.1 eV (Figure 5f). The observed signals reveal the presence of K^+ and Cl^-, respectively. It is feasible that during the long-term CO_2 reduction in $KHCO_3$ solution, an adlayer of K^+ and Cl^- forms at the Ag surface at −0.4−0.8 V.[45,60,61] This leads to gradual deposition of K^+ on the Ag surface, possibly causing a rearrangement of the surface Ag atoms[62] and finally resulting in a decrease in the surface area and in the CO_2 reduction activity. Different electronic structures of Ag 3d and Ag MVV for the Ag nanocoral sample before and after the 72 h CO_2 reduction (Table 1) could also be explained by the interaction between deposited K^+ and Cl^- with the surface Ag atoms. An additional oxidation−reduction treatment in the presence of Cl^- can restore the initial catalytic CO current efficiency.

CONCLUSION

In conclusion, we have demonstrated a simple preparation method for a chloride-modified nanoporous silver (Ag nanocoral) electrocatalyst using an oxidation−reduction process in the presence of chloride anions. The major product of CO_2 reduction on the Ag nanocorals is CO with a current efficiency of 95% at an overpotential as low as 0.37 V and a current density of 2 mA cm^{-2}. A lower limit of TOF of 0.4 s^{-1} and TON > 8.8×10^4 (over 72 h) was estimated for the Ag nanocoral catalyst at −0.6 V (vs RHE) based on the assumption that all silver atoms on the surface are catalytically active. A 32-fold increase in specific activity at −0.6 V (vs RHE) of the Ag nanocorals was observed, as compared to unmodified Ag foil, which is a greater enhancement compared to the 4-fold increase using 50 nm Ag nanoparticles. While the enhancement in the catalytic activity was previously attributed solely to a nanostructured morphology effect, hereby we propose new insights into the role of chloride anions on the increased activity of the Ag nanocoral electrocatalyst. The chloride anions not only aid in the fabrication of a high surface area nanostructured Ag electrode through an oxidation−reduction process, but are also adsorbed on the Ag surface leading to the increased intrinsic activity of CO_2 electroreduction and suppressed hydrogen evolution. Tafel analysis indicates the change in the rate-determining step from the initial electron transfer for unmodified Ag foil to the subsequent chemical step on Cl-modified Ag nanocorals. Detailed XPS studies of the Ag nanocoral catalyst revealed the presence of Cl^- anions, which are strongly bound to the surface Ag^+ ions. In addition, long-term durability tests indicate that the activity and selectivity of the Ag nanocoral catalyst decreases by only 30% over 72 h of continuous electrolysis and the original activity can be restored by an additional oxidation−reduction treatment in the presence of Cl^-. The performance degradation is attributed to a change in the morphology of the nanoporous structure and the formation of a K^+−Cl^- surface layer.

A similar oxidative−reductive treatment of silver electrodes with iodide and bromide anions results in the formation of an active surface layer, but with a different morphology than the samples produced using chloride treatment. Nevertheless, the specific activity of these samples is comparable to that of the chloride-derived Ag nanocoral electrocatalyst. Detailed mechanistic studies of the CO_2 reduction reaction using Ag electrodes modified by different halides are currently underway.

ASSOCIATED CONTENT

Supporting Information

The Supporting Information is available free of charge on the ACS Publications website at DOI: 10.1021/acscatal.5b01235.

XRD analysis of Ag foil, as-prepared AgCl, and Ag nanocorals; CO_2 reduction performance of as-prepared AgCl; SEM of Ag nanoparticles; Pb UPD of Ag electrodes treated by different methods; CO_2 reduction performance in electrolytes with different Cl^- concentrations for Ag nanocorals after annealing in H_2; CO_2 reduction performance of Ag nanoparticles with different chloride concentration; details of TON and TOF calculations for the Ag nanocoral catalyst (PDF)

AUTHOR INFORMATION

Corresponding Author

*E-mail: dep@bnl.gov.

Present Address

[†]W.X.: Advanced Photon Source, Argonne National Laboratory, 9700 S. Cass Avenue, Argonne, IL 60439.

Notes

The authors declare no competing financial interest.

ACKNOWLEDGMENTS

We thank Dr. D. C. Grills for help with preparation of this manuscript. This work was carried out at Brookhaven National Laboratory (BNL) under Contracts DE-AC02-98CH10886 and DE-SC0012704 with the U.S. Department of Energy, Office of Science, and supported in part by its Division of Chemical Sciences, Geosciences, & Biosciences within the Office of Basic Energy Sciences. The research was initiated with support from the BNL Laboratory Directed Research and Development Project No. 13-013. XPS/XRD measurements and electron microscopy were carried out at the National Synchrotron Light

DOI: 10.1021/acscatal.5b01235
ACS Catal. 2015, 5, 5349−5356

Source and the Center for Functional Nanomaterials of BNL, which are supported by the U.S. Department of Energy, Office of Basic Energy Sciences, under Contracts DE-AC02-98CH10886 and DE-SC0012704.

REFERENCES

(1) Davis, S. J.; Caldeira, K.; Matthews, H. D. *Science* **2010**, *329*, 1330−1333.
(2) Lewis, N. S.; Nocera, D. G. *Proc. Natl. Acad. Sci. U. S. A.* **2006**, *103*, 15729−15735.
(3) Asadi, M.; Kumar, B.; Behranginia, A.; Rosen, B. A.; Baskin, A.; Repnin, N.; Pisasale, D.; Phillips, P.; Zhu, W.; Haasch, R.; Klie, R. F.; Kral, P.; Abiade, J.; Salehi-Khojin, A. *Nat. Commun.* **2014**, *5*, 4470.
(4) Baturina, O. A.; Lu, Q.; Padilla, M. A.; Xin, L.; Li, W.; Serov, A.; Artyushkova, K.; Atanassov, P.; Xu, F.; Epshteyn, A.; Brintlinger, T.; Schuette, M.; Collins, G. E. *ACS Catal.* **2014**, *4*, 3682−3695.
(5) Chang, T. Y.; Liang, R. M.; Wu, P. W.; Chen, J. Y.; Hsieh, Y. C. *Mater. Lett.* **2009**, *63*, 1001−1003.
(6) Costentin, C.; Drouet, S.; Robert, M.; Saveant, J. M. *Science* **2012**, *338*, 90−94.
(7) Karamad, M.; Tripkovic, V.; Rossmeisl, J. *ACS Catal.* **2014**, *4*, 2268−2273.
(8) Kondratenko, E. V.; Mul, G.; Baltrusaitis, J.; Larrazabal, G. O.; Perez-Ramirez, J. *Energy Environ. Sci.* **2013**, *6*, 3112−3135.
(9) Kwak, J. H.; Kovarik, L.; Szanyi, J. *ACS Catal.* **2013**, *3*, 2449−2455.
(10) Lim, H. K.; Shin, H.; Goddard, W. A., 3rd; Hwang, Y. J.; Min, B. K.; Kim, H. *J. Am. Chem. Soc.* **2014**, *136*, 11355−11361.
(11) Qiao, J.; Liu, Y.; Hong, F.; Zhang, J. *Chem. Soc. Rev.* **2014**, *43*, 631−675.
(12) Schouten, K. J. P.; Pérez Gallent, E.; Koper, M. T. M. *ACS Catal.* **2013**, *3*, 1292−1295.
(13) Sen, S.; Liu, D.; Palmore, G. T. R. *ACS Catal.* **2014**, *4*, 3091−3095.
(14) Whipple, D. T.; Kenis, P. J. A. *J. Phys. Chem. Lett.* **2010**, *1*, 3451−3458.
(15) Bockris, J. O. M. *J. Electrochem. Soc.* **1989**, *136*, 2521−2528.
(16) Chandrasekaran, K.; Bockris, L. O. M. *Surf. Sci.* **1987**, *185*, 495−514.
(17) Hori, Y. In *Modern Aspects of Electrochemistry*; Vayenas, C., White, R., Gamboa-Aldeco, M., Eds.; Springer: New York, 2008; Vol. *42*, p 89−189.
(18) Schwarz, H. A.; Dodson, R. W. *J. Phys. Chem.* **1989**, *93*, 409−414.
(19) Kim, D.; Resasco, J.; Yu, Y.; Asiri, A. M.; Yang, P. *Nat. Commun.* **2014**, *5*, 4948.
(20) Li, C. W.; Ciston, J.; Kanan, M. W. *Nature* **2014**, *508*, 504−507.
(21) Li, C. W.; Kanan, M. W. *J. Am. Chem. Soc.* **2012**, *134*, 7231−7234.
(22) Reske, R.; Mistry, H.; Behafarid, F.; Roldan Cuenya, B.; Strasser, P. *J. Am. Chem. Soc.* **2014**, *136*, 6978−6986.
(23) Tang, W.; Peterson, A. A.; Varela, A. S.; Jovanov, Z. P.; Bech, L.; Durand, W. J.; Dahl, S.; Norskov, J. K.; Chorkendorff, I. *Phys. Chem. Chem. Phys.* **2012**, *14*, 76−81.
(24) Hatsukade, T.; Kuhl, K. P.; Cave, E. R.; Abram, D. N.; Jaramillo, T. F. *Phys. Chem. Chem. Phys.* **2014**, *16*, 13814−13819.
(25) Hoshi, N.; Kato, M.; Hori, Y. *J. Electroanal. Chem.* **1997**, *440*, 283−286.
(26) Lu, Q.; Rosen, J.; Zhou, Y.; Hutchings, G. S.; Kimmel, Y. C.; Chen, J. G.; Jiao, F. *Nat. Commun.* **2014**, *5*, 3242.
(27) Rosen, B. A.; Salehi-Khojin, A.; Thorson, M. R.; Zhu, W.; Whipple, D. T.; Kenis, P. J. A.; Masel, R. I. *Science* **2011**, *334*, 643−644.
(28) Salehi-Khojin, A.; Jhong, H. R. M.; Rosen, B. A.; Zhu, W.; Ma, S. C.; Kenis, P. J. A.; Masel, R. I. *J. Phys. Chem. C* **2013**, *117*, 1627−1632.
(29) Tornow, C. E.; Thorson, M. R.; Ma, S.; Gewirth, A. A.; Kenis, P. J. *J. Am. Chem. Soc.* **2012**, *134*, 19520−19523.
(30) Chen, Y.; Li, C. W.; Kanan, M. W. *J. Am. Chem. Soc.* **2012**, *134*, 19969−19972.
(31) Mistry, H.; Reske, R.; Zeng, Z.; Zhao, Z. J.; Greeley, J.; Strasser, P.; Cuenya, B. R. *J. Am. Chem. Soc.* **2014**, *136*, 16473−16476.
(32) Zhu, W.; Michalsky, R.; Metin, O.; Lv, H.; Guo, S.; Wright, C. J.; Sun, X.; Peterson, A. A.; Sun, S. *J. Am. Chem. Soc.* **2013**, *135*, 16833−16836.
(33) Peterson, A. A.; Nørskov, J. K. *J. Phys. Chem. Lett.* **2012**, *3*, 251−258.
(34) Bates, R. G.; Macaskill, J. B. *Pure Appl. Chem.* **1978**, *50*, 1701−1706.
(35) Bard, A. J.; Faulkner, L. R. *Electrochemical Methods: Fundamentals and Applications*; 2nd ed.; Wiley Global Education, 2000; p 648−650.
(36) Carro, P.; Creus, A. H.; Schilardi, P.; Gonzalez, S.; Salvarezza, R. C.; Arvia, A. J. *J. Electrochem. Soc.* **1996**, *143*, 2294−2305.
(37) Herrero, E.; Buller, L. J.; Abruna, H. D. *Chem. Rev.* **2001**, *101*, 1897−1930.
(38) Senanayake, S. D.; Mullins, D. R. *J. Phys. Chem. C* **2008**, *112*, 9744−9752.
(39) Ha, H.; Payer, J. *Electrochim. Acta* **2011**, *56*, 2781−2791.
(40) Jin, X.; Lu, J.; Liu, P.; Tong, H. *J. Electroanal. Chem.* **2003**, *542*, 85−96.
(41) Chen, J. S.; Devine, T. M.; Ogletree, D. F.; Salmeron, M. *Surf. Sci.* **1991**, *258*, 346−358.
(42) Ai, L.; Zhang, C.; Jiang, J. *Appl. Catal., B* **2013**, *142−143*, 744−751.
(43) An, C.; Wang, J.; Jiang, W.; Zhang, M.; Ming, X.; Wang, S.; Zhang, Q. *Nanoscale* **2012**, *4*, 5646−5650.
(44) Cai, B.; Wang, J.; Gan, S.; Han, D.; Wu, Z.; Niu, L. *J. Mater. Chem. A* **2014**, *2*, 5280−5286.
(45) Kautek, W.; Gordon, J. G. *J. Electrochem. Soc.* **1990**, *137*, 3405−3409.
(46) Bowker, M. *J. Electron Spectrosc. Relat. Phenom.* **1986**, *37*, 319−327.
(47) Kaushik, V. K. *J. Electron Spectrosc. Relat. Phenom.* **1991**, *56*, 273−277.
(48) Wagner, C. D.; Joshi, A. *J. Electron Spectrosc. Relat. Phenom.* **1988**, *47*, 283−313.
(49) Burstein, G. T. *Corros. Sci.* **2005**, *47*, 2858−2870.
(50) Hori, Y.; Murata, A.; Kikuchi, K.; Suzuki, S. *J. Chem. Soc., Chem. Commun.* **1987**, 728−729.
(51) Rosen, J.; Hutchings, G. S.; Lu, Q.; Rivera, S.; Zhou, Y.; Vlachos, D. G.; Jiao, F. *ACS Catal.* **2015**, *5*, 4293−4299.
(52) Gattrell, M.; Gupta, N.; Co, A. *J. Electroanal. Chem.* **2006**, *594*, 1−19.
(53) Gileadi, E.; Kirowa-Eisner, E.; Penciner, J. *Interfacial electrochemistry: an experimental approach*; Addison-Wesley Pub. Co. Advanced Book Program, 1975; p 525.
(54) Russell, P. G.; Kovac, N.; Srinivasan, S.; Steinberg, M. *J. Electrochem. Soc.* **1977**, *124*, 1329−1338.
(55) Ogura, K. *J. CO2 Util.* **2013**, *1*, 43−49.
(56) Xing, L.; Hossain, M. A.; Tian, M.; Beauchemin, D.; Adjemian, K. T.; Jerkiewicz, G. *Electrocatalysis* **2014**, *5*, 96−112.
(57) Furuya, Y.; Mashio, T.; Ohma, A.; Tian, M.; Kaveh, F.; Beauchemin, D.; Jerkiewicz, G. *ACS Catal.* **2015**, *5*, 2605−2614.
(58) Xing, L.; Jerkiewicz, G.; Beauchemin, D. *Anal. Chim. Acta* **2013**, *785*, 16−21.
(59) Gu, C.; Norris, B. C.; Fan, F.-R. F.; Bielawski, C. W.; Bard, A. J. *ACS Catal.* **2012**, *2*, 746−750.
(60) Hecht, D.; Strehblow, H. H. *J. Electroanal. Chem.* **1997**, *440*, 211−217.
(61) Lützenkirchen-Hecht, D.; Strehblow, H. H. *Electrochim. Acta* **1998**, *43*, 2957−2968.
(62) Sun, J.; He, L.; Lo, Y. C.; Xu, T.; Bi, H.; Sun, L.; Zhang, Z.; Mao, S. X.; Li, J. *Nat. Mater.* **2014**, *13*, 1007−1012.

DOI: 10.1021/acscatal.5b01235
ACS Catal. 2015, 5, 5349−5356